

1 **Dual origin of ferropericlase inclusions within super-deep diamonds**

2 Sofia Lorenzon^{a*}, Michelle Wenz^b, Paolo Nimis^a, Steven D. Jacobsen^b, Leonardo Pasqualetto^a,
3 Martha G. Pamato^a, Davide Novella^a, Dongzhou Zhang^c, Chiara Anzolini^d, Margo Regier^d, Thomas
4 Stachel^d, D. Graham Pearson^d, Jeffrey W. Harris^e and Fabrizio Nestola^a

5 *^aDepartment of Geosciences, University of Padua, Via G. Gradenigo 6, 35131 Padua, Italy*
6 *(sofia.lorenzon@phd.unipd.it, paolo.nimis@unipd.it, leonardo.pasqualetto@phd.unipd.it,*
7 *martha.pamato@unipd.it, davide.novella@unipd.it, fabrizio.nestola@unipd.it)*

8 *^bDepartment of Earth and Planetary Sciences, Northwestern University, 2145 Sheridan Rd. 60208,*
9 *Evanston, Illinois (USA) (michellewenz2020@u.northwestern.edu, s-jacobsen@northwestern.edu)*

10 *^cHawaii Institute of Geophysics and Planetology, University of Hawaii, 1680 East-West Road,*
11 *Honolulu, HI 96822, Hawaii (USA) (dzhang@hawaii.edu)*

12 *^dDepartment of Earth and Atmospheric Sciences, University of Alberta, AB T6G2E3 Edmonton,*
13 *Canada (anzolini@ualberta.ca, mregier@carnegiescience.edu, thomas.stachel@ualberta.ca,*
14 *graham.pearson@ualberta.ca)*

15 *^eSchool of Geographical and Earth Sciences, University of Glasgow, G12 8QQ Glasgow, United*
16 *Kingdom (Jeff.Harris@glasgow.ac.uk)*

17 * *Corresponding author: Sofia Lorenzon (sofia.lorenzon@phd.unipd.it)*

18 *Department of Geosciences, University of Padua,*

19 *Via G. Gradenigo 6, 35131 Padua, Italy.*

20

21

22

23 **Abstract**

24 Ferropericlasite [(Mg,Fe)O] is one of the major constituents of Earth's lower mantle and the most
25 abundant mineral inclusion in sub-lithospheric diamonds. Although a lower mantle origin for
26 ferropericlasite inclusions has often been suggested, some studies have proposed that many of these
27 inclusions may instead form at much shallower depths, in the deep upper mantle or transition zone.
28 No straightforward method exists to discriminate ferropericlasite of lower-mantle origin without
29 characteristic mineral associations, such as co-existing former bridgmanite. To explore
30 ferropericlasite-diamond growth relationships, we have investigated the crystallographic orientation
31 relationships (CORs), determined by single-crystal X-ray diffraction, between 57 ferropericlasite
32 inclusions and 37 diamonds from Juina (Brazil) and Kankan (Guinea). We show that ferropericlasite
33 inclusions can develop specific (16 inclusions in 12 diamonds), rotational statistical (9 inclusions in
34 7 diamonds) and random (32 inclusions in 25 diamond) CORs with respect to their diamond hosts.
35 All measured inclusions showing specific CORs were found to be Fe-rich ($X_{\text{FeO}} > 0.20$).
36 Coexistence of non-randomly and randomly oriented ferropericlasite inclusions within the same
37 diamond indicates that their CORs may be variably affected by local growth conditions. However,
38 the occurrence of specific CORs *only* for Fe-rich inclusions indicates that Fe-rich ferropericlasites
39 have a distinct genesis and are syngenetic with their host diamonds. This result provides strong
40 support for a dual origin for ferropericlasite in Earth's mantle, with Fe-rich compositions likely
41 indicating redox growth in the upper mantle, while more Mg-rich compositions with random COR
42 mostly representing ambient lower mantle trapped as protogenetic inclusions.

43 **Keywords:** Ferropericlasite · diamond · crystallographic orientation relationship · growth
44 relationship · syngeneses · protogeneses.

45

46

47

48 **1. Introduction**

49 Diamonds are the only natural samples through which we can investigate the mineralogy and
50 geological processes occurring in Earth's mantle at depths down to ~ 800 km depth. Most
51 information is provided by mineral and fluid inclusions entrapped by diamonds during their
52 crystallization (Meyer, 1987; Shirey et al., 2019, 2013; Weiss et al., 2015). Ferropericlasite, an oxide
53 mineral with composition ranging from MgO (periclase) and wüstite (FeO), is the most abundant
54 inclusion in super-deep diamonds, i.e., forming at sub-lithospheric depths. Experiments and
55 theoretical models on pyrolitic compositions indicate that ferropericlasite is stable in the lower
56 mantle, at depths between ~ 660 and 2900 km, and represents ~ 17% of the mantle phase
57 assemblage in a "fertile" mantle bulk composition, the remainder being represented by bridgmanite
58 (76%) and CaSiO₃-perovskite (7%) (Akaogi, 2007; Ishii et al., 2018). The predicted chemical
59 composition of lower-mantle ferropericlasite is Mg-rich, with X_{FeO} (FeO molar fraction) ranging from
60 0.08 to 0.18 (Hirose, 2002; Irifune, 1994; Ishii et al., 2018, 2011; Kuwahara et al., 2018).
61 Ferropericlasite, however, represents ~ 42% of the inclusions reported within super-deep diamonds,
62 far more abundant and showing much more variable compositions with X_{FeO} up to 0.85 than would
63 be expected for pyrolitic mantle (Walter et al., 2022 and references therein).

64 Numerous studies (see Walter et al., 2022 for a review) tried to explain these discrepancies and
65 unravel the possible geological processes involved in formation of ferropericlasite-bearing diamonds.
66 Assuming that ferropericlasite-bearing diamonds crystallized in the lower mantle, Liu (2002)
67 proposed a model according to which (Fe-rich) ferropericlasite and diamond can simultaneously
68 precipitate through decarbonation of (Mg,Fe)CO₃. Alternatively, Ryabchikov & Kaminsky (2013)
69 and Kaminsky & Lin (2017) supposed the existence of a non-pyrolitic source in the lower mantle.
70 However, experiments demonstrate that ferropericlasite can be stable in mantle rocks at depths
71 shallower than the lower mantle (Brey et al., 2004). In particular, Thomson et al. (2016) showed
72 that ferropericlasite with variable Fe contents plus diamond can crystallize simultaneously by

73 interaction between mantle peridotite and slab-derived carbonatite melts in the deep upper mantle or
74 transition zone. Therefore, in the absence of limiting characteristic mineral associations, such as the
75 presence of former bridgmanite, the depth of origin of ferropericlase-bearing diamonds remains
76 uncertain. Only inclusions associated with low-Ni enstatite, considered to be the back-
77 transformation product of bridgmanite (Stachel et al., 2000), can safely be ascribed to the lower
78 mantle. About 15% of these also co-exist with MgSiO_3 or/and CaSiO_3 phases in diamonds (Walter
79 et al., 2022).

80 Determining ferropericlase-diamond growth relationships, for instance whether the inclusion and
81 host crystallized simultaneously or whether the inclusion preceded the host, is crucial for
82 determining the possible genetic processes that formed ferropericlase-bearing diamonds.
83 Determination of crystallographic orientation relationships (CORs) for inclusion-diamond systems
84 is commonly used to derive information about their growth relationships (Milani et al., 2016;
85 Nestola et al., 2019, 2017, 2014, Nimis et al., 2019, 2018; Pamato et al., 2021; Pasqualetto et al.,
86 2022). In a preliminary study, Nimis et al. (2018) determined CORs for nine Fe-rich ($X_{\text{FeO}} \approx 0.33$ to
87 ≥ 0.64) ferropericlase inclusions in two diamonds from Juina, Brazil. These inclusions are
88 *specifically* oriented with their diamond hosts, with the principal crystallographic axes of
89 ferropericlase fixed to those of the diamond host, suggesting an epitaxial relationship. Accordingly,
90 Nimis et al. (2018) proposed that such ferropericlase nucleated during the growth history of the
91 diamond, probably by the same type of redox reactions investigated by Thomson et al. (2016) at
92 depths of the deep upper mantle or transition zone.

93 In order to increase the statistical significance of the data and to gain further insight into
94 ferropericlase-diamond growth relationships, we have determined the CORs for 57 ferropericlase
95 inclusions in 37 diamonds spanning a large compositional range to determine possible associations
96 between ferropericlase Fe-content and the depth origins of ferropericlase-bearing diamonds.

97 **2. Samples and Methods**

98 *2.1. Samples*

99 In this work, we investigated 57 ferropericlasite inclusions within 37 diamonds from two classic
100 super-deep diamond localities. A representative example of one of these diamonds is shown in Fig.
101 1. Of the investigated samples, 34 diamonds with 49 inclusions in total come from Juina, Brazil,
102 and 3 diamonds with 8 inclusions in total come from Kankan, Guinea. All the studied diamonds
103 come from alluvial deposits. They are colourless to pale yellow-brown and their size ranges from ~
104 1.5 to 5 mm. They show octahedral to irregular shapes and contain from one to four optically
105 visible and measurable ferropericlasite inclusions. The ferropericlasite inclusions, are sub-rounded to
106 irregular, 50-200 μm in size, dark in colour and show characteristic iridescence. In some specimens,
107 other mineral and fluid phases also occur (such as calcite, dolomite, magnesite, nahcolite, olivine,
108 breyite and a fluid phase similar to that reported in Nimis et al., 2016).

109 *2.2. Single-crystal X-ray diffraction*

110 X-ray diffraction data for 24 ferropericlasite inclusions and 18 diamonds were collected using a
111 Rigaku Oxford SuperNova diffractometer located at the Department of Geosciences, University of
112 Padua. This instrument is equipped with a Dectris Pilatus 200K area detector and a *Mova* X-ray
113 micro source, operating at 50 kV and 0.8 mA. The detector distance is 68 mm and the
114 diffractometer is controlled by the CrysAlis-PROTM software. Initially, each ferropericlasite inclusion
115 was centred optically and subsequently more precisely aligned by X-ray diffraction. The diffraction
116 data were collected in 360° phi-scan mode. Each frame width was 1° and the exposure time was 25-
117 60 s per frame, as a function of the inclusion size. The CrysAlis-PROTM software was also used to
118 process the collected data. By indexing the position of the diffracted peaks from the inclusions and
119 the hosts, we determined their orientation matrices, which represent the inclusion or host orientation
120 relative to the reference system of the diffractometer. Through the indexing procedure, we could
121 unambiguously distinguish diffraction peaks from ferropericlasite apart from those of diamond in the
122 same data set.

123 The remaining 33 ferropericlyase inclusions within 19 diamonds were analysed at the single-crystal
124 X-ray diffraction beamline (13-BM-C) of the GeoSoil Enviro Center for Advanced Radiation
125 Sources (GSECARS), Advanced Photon Source (APS), Argonne National Laboratory, USA. For
126 the synchrotron X-ray diffraction experiments, centering ferropericlyase inclusions in diamond was
127 facilitated using the 2D radiography attachment on beamline 13-BM-C (Wenz et al. 2019). For
128 diffraction, the X-ray beam was focused to 12 μm horizontal by 18 μm vertical at full-width half-
129 maximum. Final centering and diffraction were carried out on the six-circle goniometer following
130 the methods detailed in Zhang et al. (2017). Step scans were obtained with one-degree steps over
131 180° with an exposure time of one second per step using a MAR 165 CCD detector. Additional
132 details about the combined 2D radiography and synchrotron X-ray diffraction data collection and
133 software are reported in Wenz et al. (2019).

134 2.3. COR determination: *OrientXplot* software and misorientation distribution analysis

135 The *OrientXplot* software (Angel et al., 2015) was used to determine and plot the CORs. This
136 program processes each orientation matrix and displays a stereogram of the crystallographic
137 orientations of inclusions relative to their host, avoiding ambiguities arising from crystal symmetry.
138 In this case, both inclusions and hosts are cubic. Consequently, for each ferropericlyase-diamond
139 pair, 576 symmetrically equivalent orientations are possible. Therefore, for each inclusion-host pair,
140 we have chosen to plot the orientation for which $[1\ 1\ 0]_{\text{FPer}}$ is closest to $[1\ 1\ 0]_{\text{Dia}}$ and $[0\ 0\ 1]_{\text{FPer}}$ is
141 closest to $[0\ 0\ 1]_{\text{Dia}}$.

142 In order to determine the statistical significance of CORs in our inclusion-host systems, we carried
143 out a misorientation distribution analysis. For this purpose, we considered the angles between the
144 crystallographic axes or planes of ferropericlyase and diamond that are the most likely to form non-
145 random CORs (e.g., Nimis et al., 2019; Pasqualetto et al., 2022). The calculated misorientation
146 distributions were compared with a theoretical model of 2 million randomly oriented matrices
147 through the Kolmogorov-Smirnov test for two samples (see Wheeler et al., 2001 for more

148 information). Identification of specific, rotational statistical or random CORs was then based on the
149 presence or not of a statistically significant similarity between one or more pairs of specific
150 crystallographic directions of inclusions and hosts (Griffiths et al., 2016; Habler and Griffiths,
151 2017).

152 To increase the number of data and the statistical significance, the same procedures were extended
153 to include also two ferropericlase inclusions in diamond *AZI* previously studied by Anzolini et al.
154 (2019).

155 *2.4. Ferropericlase chemical composition*

156 The chemical compositions of three ferropericlase inclusions (inclusions in samples *AZ_08*, *AZ_15*
157 and *AZ_20*) were determined using a Tescan Solaris dual beam FE-SEM, equipped with an Ultim®
158 Max 65 EDS spectrometer. Analytical conditions were 15 keV, 3 nA, and 20 s counting time.
159 Analyses were standardised using pure oxides as standards, excepting Na, which was calibrated on
160 albite. In addition, the chemical data of four ferropericlase inclusions within *KK207* diamond were
161 collected by electron probe micro-analysis using a JEOL JXA-8900R with 5 wavelength dispersive
162 spectrometers, located at the University of Alberta. The beam energy was 20 keV energy with 30
163 nA of beam current and 2 µm diameter. The counting time was 20 seconds for Si Kα, Fe Kα, Mn
164 Kα, Ni Kα, Zn Kα, 30 seconds for V Kα, Ti Kα, Cr Kα, 40 seconds for Na Kα, K Kα, Ca Kα, Mg
165 Kα, and 120 seconds for Al Kα.

166 **3. Results**

167 *3.1. Crystallographic orientation relationships (CORs)*

168 A COR is defined as a systematic relation between the crystallographic orientations in an inclusion-
169 host system. Four types of CORs can be distinguished based on the degrees of freedom between
170 inclusion and host orientations: specific, rotational statistical, dispersional statistical and random
171 (Griffiths et al., 2016; Habler and Griffiths, 2017). This classification is only descriptive and

172 independent from the mechanisms of their formation. In specific CORs, at least two
173 crystallographic directions of the inclusion are fixed to the host (0 degrees of freedom). In rotational
174 statistical CORs, only one inclusion crystallographic orientation is fixed to that of the host (1 degree
175 of freedom). In dispersional statistical CORs, an inclusion crystallographic direction is not exactly
176 fixed to the host, but is dispersed around it within a certain misorientation angle range (2 degrees of
177 freedom, but within strict limits). In all other cases, the inclusion crystallographic directions are
178 randomly oriented relative to the host (2 degrees of freedom, with no limit).

179 The CORs for all the 57 analysed ferropericlase inclusions are shown in Fig. 2. Sixteen inclusions
180 have the three principal crystallographic axes (a_1 , a_2 , a_3) within 0-12° of those of their diamond
181 hosts (Fig. 3a). Despite the angular mismatch being in some cases greater than the measurement
182 uncertainties of $\pm 4^\circ$ (Nimis et al., 2019), all inclusions have their [1 1 2] axis within uncertainty of
183 $[1\ 1\ 2]_{\text{Dia}}$ at $< \pm 4^\circ$. These results are similar to those reported by Nimis et al. (2018) on nine
184 ferropericlase inclusions in two diamonds. As suggested by Nimis et al. (2018), the small angular
185 misorientation of the main crystallographic axes may be due to a slight rotation around the [1 1 2]
186 direction, caused by post-entrapment plastic deformation, which is well documented in super-deep
187 diamonds (e.g. Agrosi et al., 2017; Howell et al., 2012). All these inclusions are thus interpreted to
188 have been *specifically* oriented at the time of their incorporation. Another nine inclusions have their
189 [1 1 0] direction almost parallel (within $\pm 4^\circ$) to $[1\ 1\ 0]_{\text{Dia}}$ and the other crystallographic directions
190 randomly rotated around this axis (Fig. 3b). These relationships indicate a rotational statistical
191 COR. The remaining inclusions (32 inclusions in 25 diamonds) do not show any particular
192 crystallographic orientation with respect to their hosts (Fig. 3c). The statistical significance of the
193 observed specific and rotational statistical CORs was tested by comparing the observed
194 misorientation angle distributions against a theoretical random distribution (Kolmogorov-Smirnov
195 test for two samples, $p < 0.001$).

196 Diamonds containing more than one ferropericlaase inclusion (13 out of 37 diamonds) showed
197 further interesting features. In three of these samples (*5a08*, *5a26*, *5a27*), inclusions that are
198 specifically oriented coexist with others that are randomly oriented (Fig. 4a). Diamond *5a06*
199 contains one specifically oriented inclusion and one that suggests a rotational statistical COR (Fig.
200 4b). In diamonds *5a04* and *6b23*, one inclusion with a rotational statistical COR and one randomly
201 oriented inclusion coexist (Fig. 4c). Finally, in four diamonds (*KK34*, *KK207*, *6a05*, *6b17*) more
202 than one inclusion share a similar orientation, but they are randomly oriented relative to their
203 diamond hosts (Fig. 5).

204 *3.2. Ferropericlaase chemical composition*

205 The chemical compositions of ferropericlaase inclusions in diamond *AZ_08* (1 inclusion), *AZ_15* (1
206 inclusion), *AZ_20* (1 inclusion) and *KK207* (4 inclusions) are reported in Table 1. The X_{FeO} fraction
207 ranges from 0.14 to 0.32. Previous data for other crystallographically analysed ferropericlaase
208 inclusions in diamonds studied by (Anzolini et al., 2019) and Nimis et al. (2018) are reported in the
209 same Table.

210 **Discussion**

211 Our analysis of 57 ferropericlaase inclusions within 37 diamonds shows that ferropericlaase can
212 develop specific (16 inclusions in 12 diamonds), rotational statistical (9 inclusions in 7 diamonds)
213 and random (32 inclusions in 25 diamonds) CORs with respect to their diamond hosts. Non-random
214 (i.e., specific and rotational statistical) CORs indicate that mechanical or surface interaction
215 occurred between ferropericlaase and diamond during formation of the inclusion-host system (Habler
216 and Griffiths, 2017; Wheeler et al., 2001). Mechanical juxtaposition of two well-shaped crystals is
217 most likely to generate rotational statistical CORs, in which the two crystals share the axes normal
218 to the juxtaposed faces (Nimis et al., 2019; Wheeler et al., 2001). In our samples characterised by
219 rotational statistical COR, ferropericlaase and diamond share a common [1 1 0] axis. If the driving
220 force for this COR was mechanical, this would imply juxtaposition of the {1 1 0} faces of both

221 minerals. Although ferropericlase and diamond can rarely develop $\{1\ 1\ 0\}$ faces during their growth
222 (Koretsky et al., 1998; Sunagawa, 1990), their crystals commonly have octahedral habits with well-
223 formed $\{1\ 1\ 1\}$ faces. Consequently, one would expect to observe frequent rotational statistical
224 CORs around $[1\ 1\ 1]$ and not around $[1\ 1\ 0]$. Therefore, we do not favour a role of mechanical
225 interaction in the development of rotational statistical CORs in our samples.

226 Surface interaction may also cause the development of non-random CORs (Wheeler et al., 2001). In
227 fact, under favourable conditions, two mineral grains may align their crystal lattices or one of their
228 lattice directions to minimize their interface energy. Nimis et al. (2018) discussed the possible
229 scenarios that could lead to crystallographic alignment between inclusion and host by surface
230 interaction in super-deep diamonds. These scenarios include (1) grain rotation during static
231 recrystallization, or (2) mutual growth or epitaxial nucleation during crystallization from a fluid or
232 melt. Scenario 1 was considered to be highly unlikely, given the high-stress environment in which
233 super-deep diamonds form. Scenario 2 implies precipitation of the included minerals during the
234 growth history of diamond and we suggest may apply to all investigated ferropericlase-diamond
235 pairs showing non-random CORs.

236 Coexistence of non-random and random CORs in some of the studied diamonds (Fig. 4) is not in
237 conflict with the above interpretation, since local physical-chemical and stress conditions may
238 affect the efficiency of surface interactions (Mutaftschiev, 2001; Wheeler et al., 2001). Therefore,
239 the absence of a non-random COR should not be considered as evidence against contemporaneous
240 growth. Also, a rotational statistical CORs could reflect a “starting preferred crystallographic
241 orientation” between ferropericlase and diamond. This would explain the coexistence in some of
242 our samples of rotational statistical and either specific or random CORs within the same diamond.

243 Four diamonds each contain pairs of ferropericlase inclusions, which are iso-oriented with respect
244 to each other, but are randomly oriented with respect to their diamond hosts (Fig. 5). In one of
245 these, diamond *6b17*, $[1\ 1\ 0]_{\text{FPer}}$ is 4° from $[1\ 1\ 0]_{\text{Dia}}$, but this relatively small misalignment may

246 well represent just one of an infinite number of possible random orientations. Inclusion iso-
247 orientation without a specific COR with the diamond host is considered to be evidence of a
248 protogenetic origin of the inclusions (Milani et al., 2016; Nestola et al., 2014; Nimis et al., 2019;
249 Pamato et al., 2021; Pasqualetto et al., 2022).

250 Our compilation of ferropericlyase inclusions for which both CORs and chemical data are available
251 (Anzolini et al., 2019; Nimis et al., 2018; and present study) (Table 1) indicates a strong
252 relationship between ferropericlyase Fe content and ferropericlyase-diamond growth relationships.
253 Almost all (12 out of 13) Fe-rich ferropericlyase inclusions ($X_{\text{FeO}} > 0.2$) present specific CORs.
254 Evaluating the relationship between the Fe-rich composition of ferropericlyase and the development
255 of specific COR through a not-parametric statistical test (Fisher's exact test), we have obtained very
256 low probabilities ($p < 0.001$) that the presence of this specific COR is independent from the Fe-rich
257 composition of ferropericlyase within the studied population. This indicates that the association
258 between these two parameters is highly statistically significant. On the other hand, 4 out of 5 Mg-
259 rich ferropericlyase inclusions with $X_{\text{FeO}} < 0.2$ present random CORs, while the remaining one is
260 compatible with both a random and a rotational statistical COR. In diamond *KK207*, multiple Mg-
261 rich inclusions show evidence of a protogenetic origin (Fig. 5). Moreover, the reported Mg-rich
262 ferropericlyase inclusions have chemical compositions similar to those of ferropericlyases in
263 association with former bridgmanite within diamonds (n=33, X_{FeO} ranging ~0.10 to 0.31 and one
264 sample having $X_{\text{FeO}} \sim 0.35$, Davies et al., 2004; Harte and Harris, 1994; Hayman et al., 2005;
265 Stachel et al., 2000; Tappert et al., 2009). Note that ferropericlyases with $X_{\text{FeO}} > 0.2$ are not in
266 chemical equilibrium with co-existing former bridgmanite and these were probably entrapped
267 during different diamond growth events, reflecting different chemical environments in Earth's
268 mantle (Harte and Harris, 1994; Hayman et al., 2005). These results strongly suggest that Fe-rich
269 and Fe-poor ferropericlyases generally form by distinct processes under distinct conditions.

270 We suggest that Fe-rich ferropericlasite inclusions, which frequently present specific CORs, are
271 syngenetic with their diamond hosts and were formed in the deep upper mantle or transition zone by
272 redox processes similar to those reproduced in Thomson et al.'s (2016) experiments (Fig. 6a).
273 Conversely, Mg-rich ferropericlasite inclusions, which have chemical compositions similar to those
274 of ferropericlasites associated with low-Ni enstatite (evidence of a lower mantle origin; Davies et al.,
275 2004; Harte and Harris, 1994; Hayman et al., 2005; Stachel et al., 2000; Tappert et al., 2009) and
276 those predicted for lower-mantle ferropericlasite (Akaogi, 2007; Ishii et al., 2018), present random
277 CORs, and in some cases show clear evidence of protogenesis. Consequently, we propose that these
278 Mg-rich ferropericlasites represent parts of pre-existing mineral assemblages, which were partially
279 dissolved and passively entrapped by diamond during its precipitation in the lower mantle (Fig. 6b).
280 These results thus allow future geochemical studies of ferropericlasite to confidently distinguish
281 those formed at relatively shallow mantle levels by slab mantle interaction from those likely present
282 in the upper mantle before diamond crystallisation and entrapment. The observed relationships
283 indicate that Fe-rich ferropericlasite is unlikely to reflect a typical upper or lower mantle
284 composition.

285 **Conclusions**

286 The results of this study can be summarised as follows.

- 287 1) The determination of the relative crystallographic orientations of 57 ferropericlasite
288 inclusions in 37 diamonds revealed the occurrence of specific, rotational statistical and
289 random CORs.
- 290 2) A non-random COR is typical of Fe-rich ($X_{\text{FeO}} > 0.2$) ferropericlasite inclusions, whereas Fe-
291 poor ($X_{\text{FeO}} < 0.2$) ferropericlasite inclusions show random CORs and sometimes exhibit clear
292 evidence of protogenesis.

- 293 3) Fe-rich ferropericlasite inclusions presenting non-random CORs are interpreted to have been
294 formed together with their host diamonds in the deep upper mantle or transition zone,
295 probably by interaction of mantle peridotite with slab-derived carbonatite melts.
- 296 4) Mg-rich ferropericlasite inclusions presenting random CORs could be remnants of pre-
297 existing mineral assemblages, which were entrapped by the growing diamonds in the lower
298 mantle.

299 The dual origin of ferropericlasite inclusions in diamonds (Fe-poor protogenetic vs. Fe-rich
300 syngenetic) provides a simple explanation for the observed discrepancies between theoretical
301 mineralogical models for the lower mantle and the relative abundance and composition of
302 ferropericlasite inclusions in diamonds.

303 **CRedit author statement**

304 **Sofia Lorenzon:** Conceptualization, Investigation, Formal analysis, Writing – Original Draft
305 **Michelle Wenz:** Investigation, Formal analysis, Writing – Review & Editing **Paolo Nimis:**
306 Conceptualization, Investigation, Writing – Review & Editing **Steven D. Jacobsen:**
307 Conceptualization, Funding acquisition, Writing – Review & Editing **Leonardo Pasqualetto:**
308 Formal analysis, Writing – Review & Editing **Martha G. Pamato:** Funding acquisition, Writing –
309 Review & Editing **Davide Novella:** Funding acquisition, Writing & Editing **Dongzhou Zhang:**
310 Investigation **Chiara Anzolini:** Writing – Review & Editing **Margo Regier:** Investigation **Thomas**
311 **Stachel:** Resources, Writing – Review & Editing **D. Graham Pearson:** Resources, Writing –
312 Review & Editing **Jeffrey W. Harris:** Resources, Writing – Review & Editing **Fabrizio Nestola:**
313 Conceptualization, Resources, Supervision, Funding acquisition, Writing – Review & Editing.

314 **Declaration of Competing Interest**

315 The authors declare that they have no known competing financial interests or personal relationships
316 that could have appeared to influence the work reported in this paper.

317 **Acknowledgements**

318 FN thanks the European Research Council (grant agreement n. 307322). DN thanks the Rita Levi
319 Montalcini programme (Italian Ministry of University and Research) for support. This study was
320 also supported in part through the U.S. National Science Foundation (NSF) grant EAR-1853521 to
321 SDJ. Portions of this work were performed at GeoSoilEnviroCARS (The University of Chicago,
322 Sector 13), Advanced Photon Source (APS), Argonne National Laboratory. GeoSoilEnviroCARS is
323 supported by NSF grant EAR-1634415. This research used resources of the APS, a U.S.
324 Department of Energy (DOE) Office of Science User Facility operated for the DOE Office of
325 Science by Argonne National Laboratory under Contract No. DE-AC02-06CH11357. Experiments
326 at beamline 13-BM-C used the PX² facility, supported by COMPRES under NSF Cooperative
327 Agreement EAR-1661511.

328 **References**

- 329 Akaogi, M., 2007. Phase transitions of minerals in the transition zone and upper part of the lower
330 mantle. *Spec. Pap. Geol. Soc. Am.* 421, 1–13. [https://doi.org/10.1130/2007.2421\(01\)](https://doi.org/10.1130/2007.2421(01))
- 331 Anzolini, C., Nestola, F., Mazzucchelli, M.L., Alvaro, M., Nimis, P., Gianese, A., Morganti, S.,
332 Marone, F., Campione, M., Hutchison, M.T., Harris, J.W., 2019. Depth of diamond formation
333 obtained from single periclase inclusions. *Geology* 47, 219–222.
334 <https://doi.org/10.1130/G45605.1>
- 335 Brey, G.P., Bulatov, V., Gurnis, A., Harris, J.W., Stachel, T., 2004. Ferropericlase - A lower mantle
336 phase in the upper mantle. *Lithos* 77, 655–663. <https://doi.org/10.1016/j.lithos.2004.03.013>
- 337 Davies, R.M., Griffin, W.L., O'Reilly, S.Y., Doyle, B.J., 2004. Mineral inclusions and geochemical
338 characteristics of microdiamonds from the DO27, A154, A21, A418, DO18, DD17 and Ranch
339 Lake kimberlites at Lac de Gras, Slave Craton, Canada. *Lithos* 77, 39–55.
340 <https://doi.org/10.1016/j.lithos.2004.04.016>

341 Griffiths, T.A., Habler, G., Abart, R., 2016. Crystallographic orientation relationships in host-
342 inclusion systems: New insights from large EBSD data sets. *Am. Mineral.* 101, 690–705.
343 <https://doi.org/10.2138/am-2016-5442>

344 Habler, G., Griffiths, T.A., 2017. Crystallographic orientation relationships. *EMU Notes Mineral.*
345 16, 541–585.

346 Harte, B., Harris, J.W., 1994. Lower mantle mineral associations preserved in diamonds. *Mineral.*
347 *Mag.* 58A, 384–385. <https://doi.org/10.1180/minmag.1994.58A.1.201>

348 Hayman, P.C., Kopylova, M.G., Kaminsky, F. V., 2005. Lower mantle diamonds from Rio Soriso
349 (Juina area, Mato Grosso, Brazil). *Contrib. to Mineral. Petrol.* 149, 430–445.
350 <https://doi.org/10.1007/s00410-005-0657-8>

351 Hirose, K., 2002. Phase transitions in pyrolitic mantle around 670-km depth: Implications for
352 upwelling of plumes from the lower mantle. *J. Geophys. Res. Solid Earth* 107, ECV 3-1-ECV
353 3-13. <https://doi.org/10.1029/2001jb000597>

354 Irifune, T., 1994. Absence of an aluminous phase in the upper part of the Earth's lower mantle.
355 *Nature* 370, 131–133. <https://doi.org/10.1038/370131a0>

356 Ishii, T., Kojitani, H., Akaogi, M., 2018. Phase relations and mineral chemistry in pyrolitic mantle
357 at 1600–2200 °C under pressures up to the uppermost lower mantle: Phase transitions around
358 the 660-km discontinuity and dynamics of upwelling hot plumes. *Phys. Earth Planet. Inter.*
359 274, 127–137. <https://doi.org/10.1016/j.pepi.2017.10.005>

360 Ishii, T., Kojitani, H., Akaogi, M., 2011. Post-spinel transitions in pyrolite and Mg₂SiO₄ and
361 akimotoite-perovskite transition in MgSiO₃: Precise comparison by high-pressure high-
362 temperature experiments with multi-sample cell technique. *Earth Planet. Sci. Lett.* 309, 185–
363 197. <https://doi.org/10.1016/j.epsl.2011.06.023>

364 Koretsky, C.M., Sverjensky, D.A., Sahai, N., 1998. A model of surface site types on oxide and
365 silicate minerals based on crystal chemistry: implication for site types and densities, multi-site
366 adsorption, surface infrared spectroscopy, and dissolution kinetics. *Am. J. Sci.* 298, 349–438.

367 Kuwahara, H., Nomura, R., Nakada, R., Irifune, T., 2018. Simultaneous determination of melting
368 phase relations of mantle peridotite and mid-ocean ridge basalt at the uppermost lower mantle
369 conditions. *Phys. Earth Planet. Inter.* 284, 36–50. <https://doi.org/10.1016/j.pepi.2018.08.012>

370 Liu, L. gun, 2002. An alternative interpretation of lower mantle mineral associations in diamonds.
371 *Contrib. to Mineral. Petrol.* 144, 16–21. <https://doi.org/10.1007/s00410-002-0389-y>

372 Milani, S., Nestola, F., Angel, R.J., Nimis, P., Harris, J.W., 2016. Crystallographic orientations of
373 olivine inclusions in diamonds. *Lithos* 265, 312–316.
374 <https://doi.org/10.1016/j.lithos.2016.06.010>

375 Nestola, F., Jacob, D.E., Pamato, M.G., Pasqualetto, L., Oliveira, B., Greene, S., Perritt, S., Chinn,
376 I., Milani, S., Kueter, N., Sgreva, N., Nimis, P., Secco, L., Harris, J.W., 2019. Protogenetic
377 garnet inclusions and the age of diamonds. *Geology* 47, 431–434.
378 <https://doi.org/10.1130/G45781.1>

379 Nestola, F., Jung, H., Taylor, L.A., 2017. Mineral inclusions in diamonds may be synchronous but
380 not syngenetic. *Nat. Commun.* 8, 6–11. <https://doi.org/10.1038/ncomms14168>

381 Nestola, F., Nimis, P., Angel, R.J., Milani, S., Bruno, M., Prencipe, M., Harris, J.W., 2014. Olivine
382 with diamond-imposed morphology included in diamonds. Syngenesi or protogenesis? *Int.*
383 *Geol. Rev.* 56, 1658–1667. <https://doi.org/10.1080/00206814.2014.956153>

384 Nimis, P., Alvaro, M., Nestola, F., Angel, R.J., Marquardt, K., Rustioni, G., Harris, J.W., Marone,
385 F., 2016. First evidence of hydrous silicic fluid films around solid inclusions in gem-quality
386 diamonds. *Lithos* 260, 384–389. <https://doi.org/10.1016/j.lithos.2016.05.019>

387 Nimis, P., Angel, R.J., Alvaro, M., Nestola, F., Harris, J.W., Casati, N., Marone, F., 2019.
388 Crystallographic orientations of magnesiochromite inclusions in diamonds: what do they tell
389 us? *Contrib. to Mineral. Petrol.* 174, 1–13. <https://doi.org/10.1007/s00410-019-1559-5>

390 Nimis, P., Nestola, F., Schiazza, M., Reali, R., Agrosi, G., Mele, D., Tempesta, G., Howell, D.,
391 Hutchison, M.T., Spiess, R., 2018. Fe-rich ferropicrinite and magnesiochromite inclusions
392 reflecting diamond formation rather than ambient mantle. *Geology* 47, 27–30.
393 <https://doi.org/10.1130/G45235.1>

394 Pamato, M.G., Novella, D., Jacob, D.E., Oliveira, B., Pearson, D.G., Greene, S., Afonso, J.C.,
395 Favero, M., Stachel, T., Alvaro, M., Nestola, F., 2021. Protogenetic sulfide inclusions in
396 diamonds date the diamond formation event using Re-Os isotopes. *Geology* 49, 941–945.
397 <https://doi.org/10.1130/G48651.1>

398 Pasqualetto, L., Nestola, F., Jacob, D.E., Pamato, M.G., Oliveira, B., Perritt, S., Chinn, I., Nimis, P.,
399 Milani, S., Harris, J.W., 2022. Protogenetic clinopyroxene inclusions in diamond and Nd
400 diffusion modeling—Implications for diamond dating. *Geology* XX, 1–5.
401 <https://doi.org/10.1130/g50273.1>

402 Ryabchikov, I.D., Kaminsky, F. V., 2013. The composition of the lower mantle: Evidence from
403 mineral inclusions in diamonds. *Dokl. Earth Sci.* 453, 1246–1249.
404 <https://doi.org/10.1134/S1028334X13120155>

405 Shirey, S.B., Cartigny, P., Frost, D.J., Keshav, S., Nestola, F., Nimis, P., Pearson, D.G., Sobolev, N.
406 V., Walter, M.J., 2013. Diamonds and the Geology of Mantle Carbon. *Rev. Mineral.*
407 *Geochemistry* 75, 355–421. <https://doi.org/10.2138/rmg.2013.75.12>

408 Shirey, S.B., Smit, K. V., Pearson, D.G., Walter, M.J., Aulbach, S., Brenker, F.E., Bureau, H.,
409 Burnham, A.D., Cartigny, P., Chacko, T., Frost, D.J., Hauri, E.H., Jacob, D.E., Jacobsen, S.D.,
410 Kohn, S.C., Luth, R.W., Mikhail, S., Navon, O., Nestola, F., Nimis, P., Palot, M., Smith, E.M.,

411 Stachel, T., Stagno, V., Steele, A., Stern, R.A., Thomassot, E., Thomson, A.R., Weiss, Y.,
412 2019. Diamonds and the mantle geodynamics of carbon: deep mantle carbon evolution from
413 the diamond record, *Deep Carbon: Past to Present*.
414 <https://doi.org/10.1017/9781108677950.005>

415 Stachel, T., Harris, J.W., Brey, G.P., Joswig, W., 2000. Kankan diamonds (Guinea) II: Lower
416 mantle inclusion parageneses. *Contrib. to Mineral. Petrol.* 140, 16–27.
417 <https://doi.org/10.1007/s004100000174>

418 Sunagawa, I., 1990. Growth and morphology of diamond crystals under stable and metastable
419 conditions. *J. Cryst. Growth* 99, 1156–1161.

420 Tappert, R., Foden, J., Stachel, T., Muehlenbachs, K., Tappert, M., Wills, K., 2009. The diamonds
421 of South Australia. *Lithos* 112, 806–821. <https://doi.org/10.1016/j.lithos.2009.04.029>

422 Thomson, A.R., Walter, M.J., Kohn, S.C., Brooker, R.A., 2016. Slab melting as a barrier to deep
423 carbon subduction. *Nature* 529, 76–79. <https://doi.org/10.1038/nature16174>

424 Walter, M.J., Thomson, A.R., Smith, E.M., 2022. Geochemistry of Silicate and Oxide Inclusions in
425 Sublithospheric Diamonds. *Rev. Mineral. Geochemistry* 88, 393–450.
426 <https://doi.org/10.2138/rmg.2022.88.07>

427 Weiss, Y., McNeill, J., Pearson, D.G., Nowell, G.M., Ottley, C.J., 2015. Highly saline fluids from a
428 subducting slab as the source for fluid-rich diamonds. *Nature* 524, 339–342.
429 <https://doi.org/10.1038/nature14857>

430 Wenz, M.D., Jacobsen, S.D., Zhang, D., Regier, M., Bausch, H.J., Dera, P.K., Rivers, M., Eng, P.,
431 Shirey, S.B., Pearson, D.G., 2019. Fast identification of mineral inclusions in diamond at
432 GSECARS using synchrotron X-ray microtomography, radiography and diffraction. *J.*
433 *Synchrotron Radiat.* 26, 1763–1768. <https://doi.org/10.1107/S1600577519006854>

434 Wheeler, J., Prior, D.J., Jiang, Z., Spiess, R., Trimby, P.W., 2001. The petrological significance of
435 misorientations between grains. *Contrib. to Mineral. Petrol.* 141, 109–124.
436 <https://doi.org/10.1007/s004100000225>

437 Zhang, D., Dera, P.K., Eng, P.J., Stubbs, J.E., Zhang, J.S., Prakapenka, V.B., Rivers, M.L., 2017.
438 High pressure single crystal diffraction at PX². *J. Vis. Exp.* 2017, 1–9.
439 <https://doi.org/10.3791/54660>

440

441

442

443

444

445

446

447

448

449

450

451

452

453

454

455 **Figures**

456 Figure 1. One of the studied ferropericlyase-bearing diamonds (AZ_08) under incident light. This
457 specific sample comes from Juina (Brazil), is pale-yellow and has an elongated irregular shape. The
458 ferropericlyase inclusion (within the red circle and indicated by the red arrow) is dark in colour and
459 ~250 μm sized.



460

461

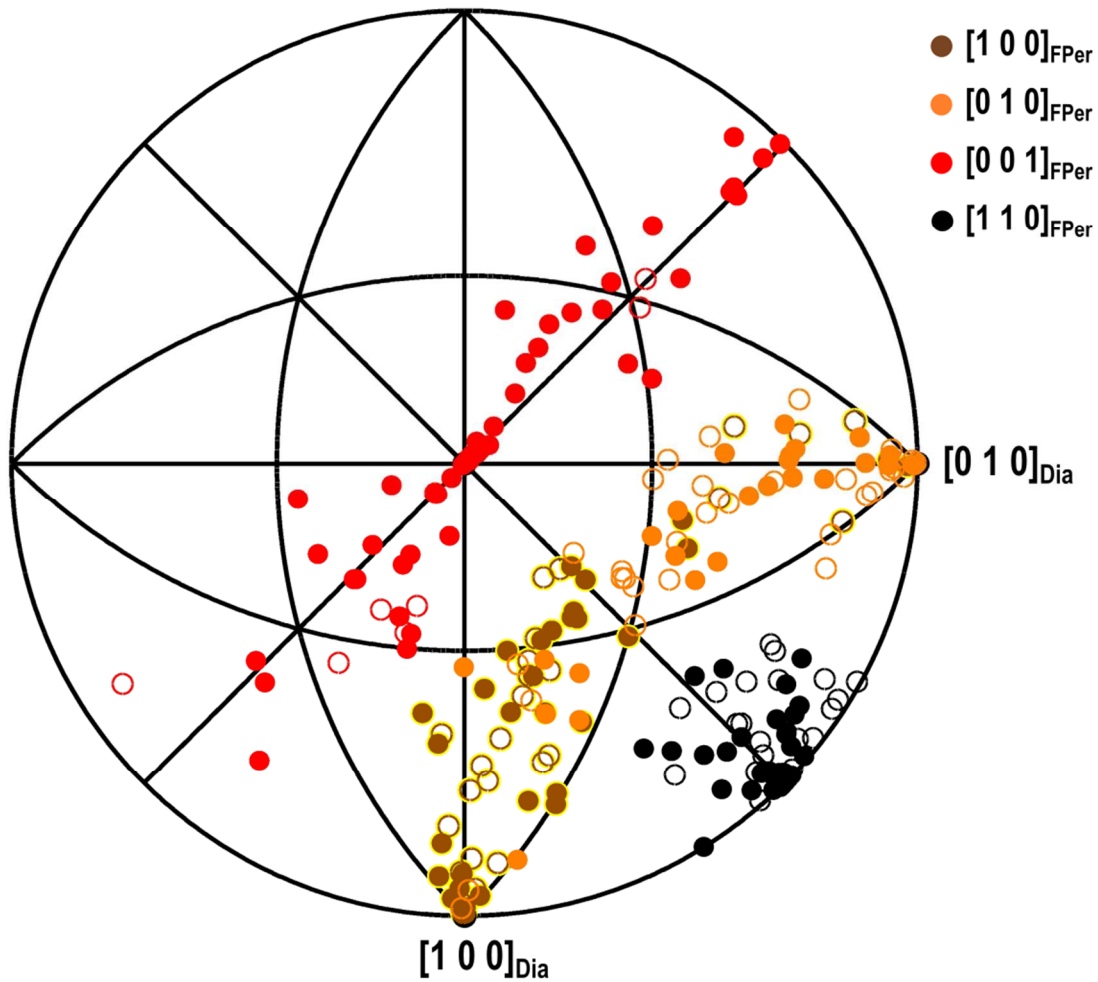
462

463

464

465

466 Figure 2. Crystallographic orientation relationships (CORs) between all analysed 57 ferropericlasite
467 inclusions and their 37 diamond hosts, plotted using OrientXplot software (Angel et al., 2015).
468 Open symbols plot in the lower hemisphere.



469

470

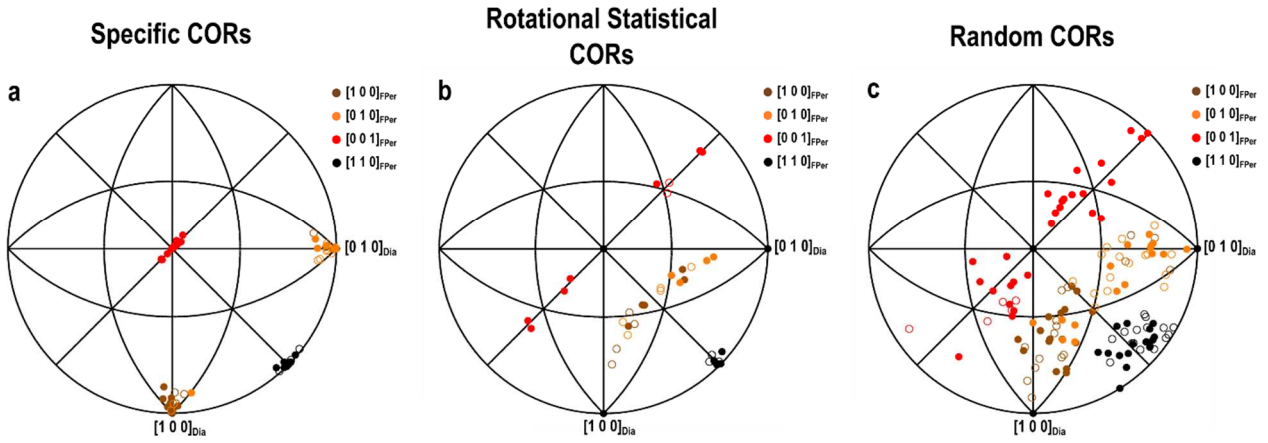
471

472

473

474

475 Figure 3. Stereographic projections showing ferropericlaase inclusions presenting a) specific CORs
 476 (16 inclusions in 12 diamonds), b) rotational statistical CORs ($[1\ 1\ 0]_{\text{FPer}} // [1\ 1\ 0]_{\text{Dia}}$, 9 inclusions in
 477 7 diamonds) and c) random CORs (32 inclusions in 25 diamonds) relative to their diamond hosts.



478

479

480

481

482

483

484

485

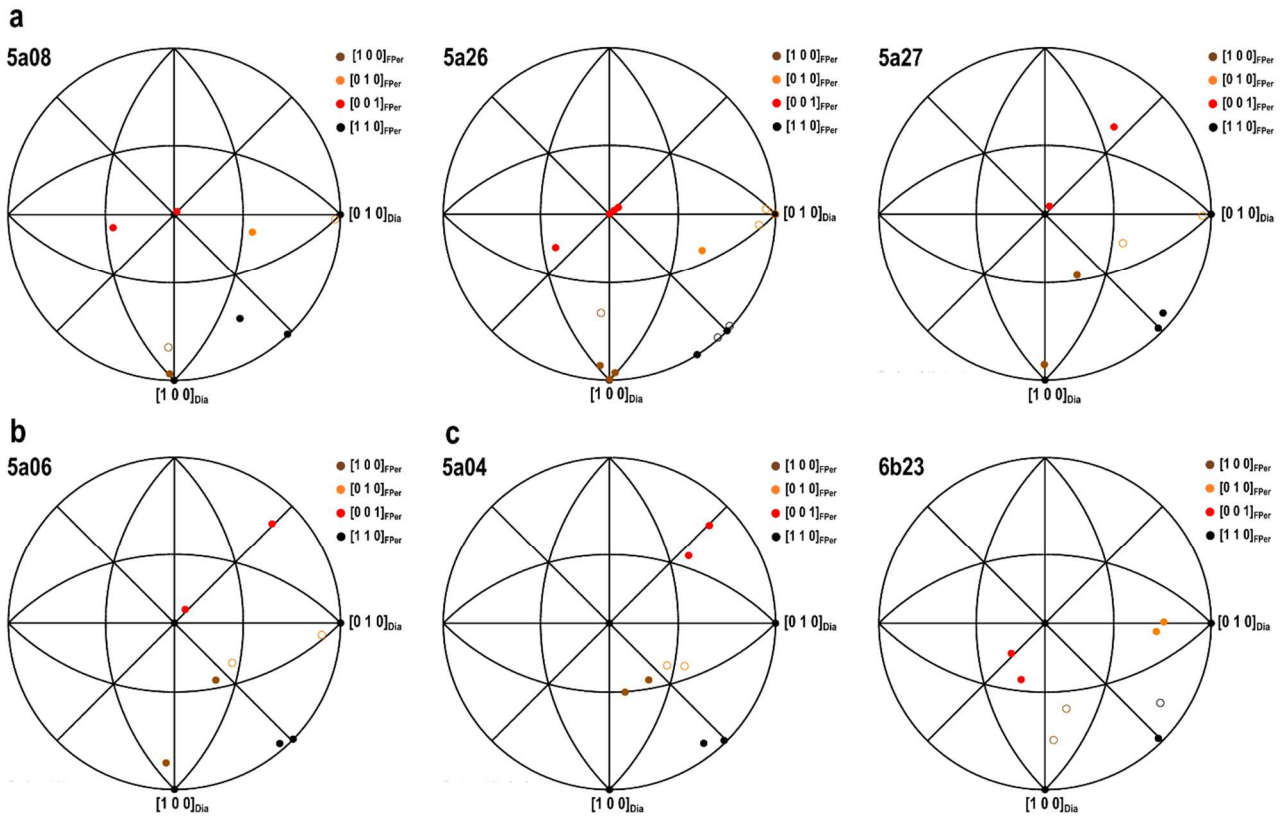
486

487

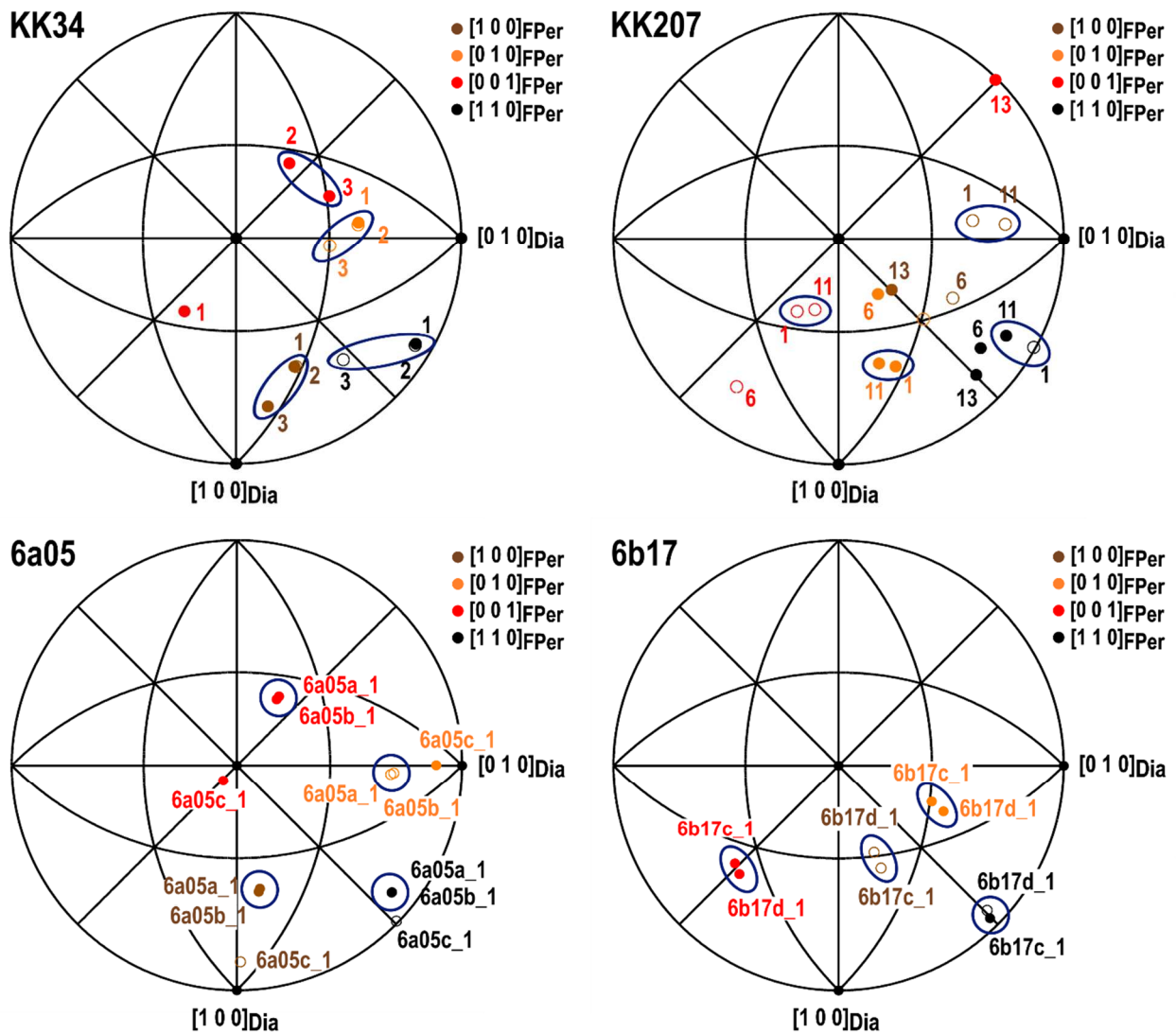
488

489

490 Figure 4. Stereographic projections of diamonds containing ferropericlae inclusions which present
 491 a) both specific and random CORs (5a08, 5a26, 5a27), b) both specific and rotational statistical
 492 CORs (5a06) and c) both rotational statistical and random CORs (5a04, 6b23) relative to their
 493 diamond hosts.



502 Figure 5. Crystallographic orientation relationships (CORs) of ferropericase inclusions within
 503 *KK34*, *KK207*, *6a05* and *6b17* diamonds. Multiple ferropericase inclusions are defined by the
 504 numbers close to dots (i.e. 1, 2,...). Blue circles indicate the ferropericase inclusions presenting
 505 similar CORs, but different and random CORs to their diamond host. These inclusions are
 506 protogenetic, representing remnant parts of pre-existing mono-crystals that were dissolved and
 507 entrapped during diamond precipitation.



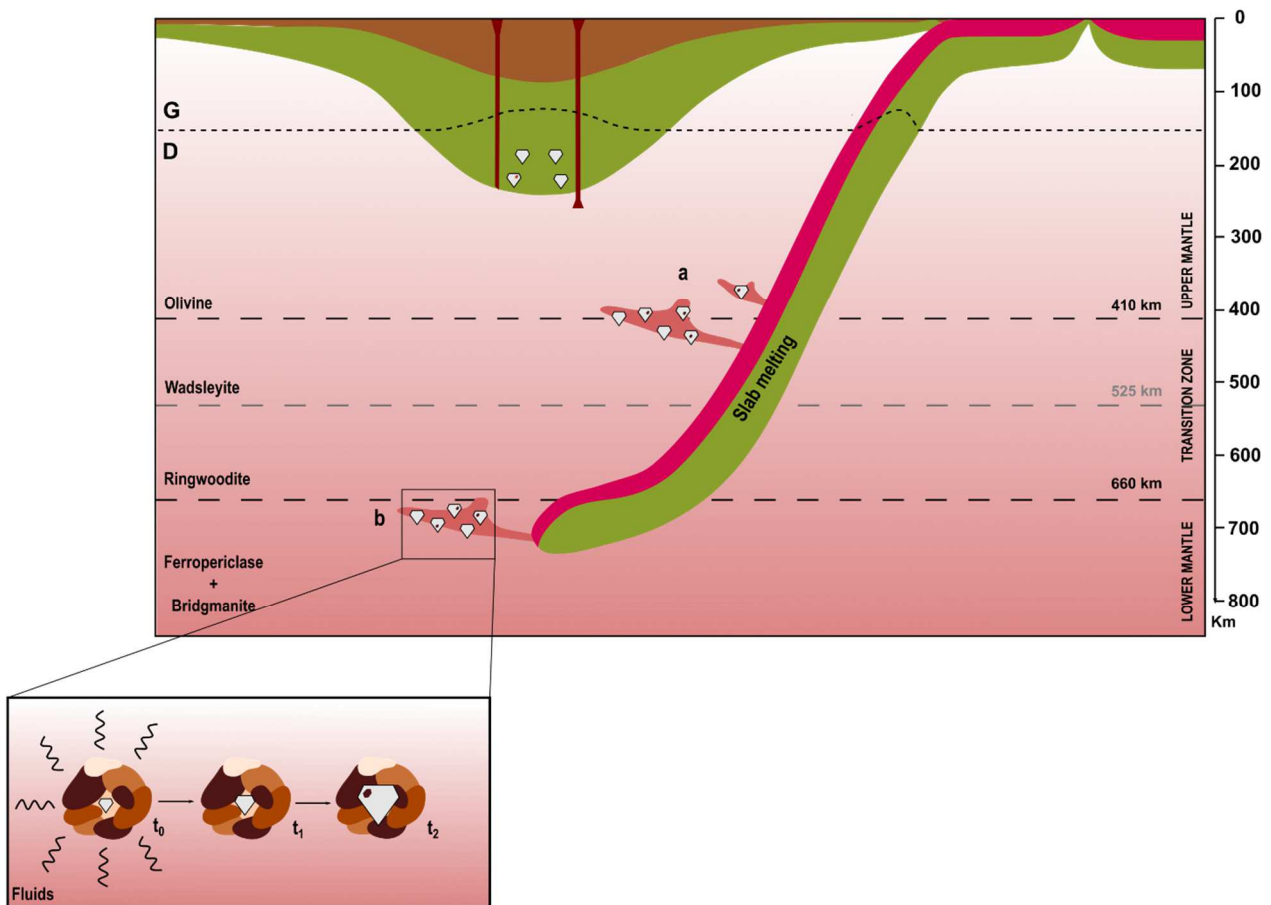
508

509

510

511

512 Figure 6. Possible scenarios for the formation of Fe-rich and Fe-poor ferropericlase-bearing
 513 diamonds in Earth's mantle. a) Precipitation of diamonds and Fe-rich ferropericlase due to reactions
 514 between slab-derived carbonatite melts and peridotitic rocks, at depths of the deep upper mantle or
 515 of the transition zone (Thomson et al., 2016). In this case, the ferropericlase inclusions are
 516 syngenetic and generally develop specific CORs with their diamond hosts. b) Formation of
 517 diamonds in the uppermost lower mantle. In this case, pre-existing Mg-rich ferropericlase
 518 inclusions are partially dissolved and passively incorporated into the growing diamonds, without
 519 development of particular CORs. Multiple inclusions in individual diamonds may be iso-oriented if
 520 they are derived from the same original ferropericlase grain. Only in this case do the inclusions
 521 have chemical compositions similar to those experimentally predicted for ferropericlase in the lower
 522 mantle.



523

524

525

526 **Tables**

527 Table 1. Chemical composition and interpreted COR of ferropericlase inclusions.

	Diamond	Inclusion	Chemical composition	Type of COR
Nimis et al. 2018	BZ270	1	(Mg _{0.66} Fe _{0.34})O	Specific
		2	(Mg _{0.65} Fe _{0.35})O	Specific
		3	(Mg _{0.65} Fe _{0.35})O	Specific
		4	(Mg _{0.65} Fe _{0.35})O	Specific
		5	(Mg _{0.66} Fe _{0.34})O	Specific
	JUc4	1	(Mg _{0.43} Fe _{0.57})O	Specific
		2	(Mg _{0.56} Fe _{0.44})O	Specific
		3	(Mg _{0.57} Fe _{0.43})O	Specific
4		(Mg _{0.36} Fe _{0.64})O	Specific	
Anzolini et al. 2019	AZ1	AZ1_1	(Mg _{0.61} Fe _{0.39})O	Specific
		AZ1_2	(Mg _{0.59} Fe _{0.41})O	Specific
This study	AZ_08	AZ_08_01	(Mg _{0.68} Fe _{0.32})O	Random
	AZ_15	AZ_15_01	(Mg _{0.80} Fe _{0.20})O	Random
	AZ_20	AZ_20_01	(Mg _{0.69} Fe _{0.31})O	Specific
	KK207	1	(Mg _{0.86} Fe _{0.14})O	Random
		6	(Mg _{0.86} Fe _{0.14})O	Random
		11	(Mg _{0.86} Fe _{0.14})O	Random
		13	(Mg _{0.86} Fe _{0.14})O	Rotational statistical

528

529